INSIGHTS ON SURFACE ANALYSIS TECHNIQUES TO STUDY GLASS PRIMARY PACKAGING

GIOVANNA PINTORI[1,2]*, SERENA PANIGHELLO[1], ODRA PINATO[1], ELTI CATTARUZZA[2]

[1] EMEA Technology Excellence Center, Stevanato Group, via Molinella 17, Piombino Dese, 35017, Italy.

[2] Department of Molecular Sciences and Nanosystems, Ca' Foscari University of Venice, via Torino 155, Venezia-Mestre, 30172, Italy

ABSTRACT

During the forming process of a vial by tubing glass, temperatures of up to 1200°C are applied to adjust the glass viscosity. This process causes the release of volatile components such as alkali borates. Consequently, the percentage of sodium and boron measured on the inner surface of the vial can be higher than that measured on the corresponding glass tube.

This study aimed to characterize the inner surface of two different type I borosilicate glass tubes before and after the vial forming process at the nanoscale level. Quantitative elemental analysis of the surface along the vertical axis of glass tubes and vials was performed by X-ray Photoelectron Spectroscopy (XPS), while the topographical investigation was carried out by Scanning Electron Microscopy (SEM). In the near-bottom region of a vial, which is usually the area most prone to corrosion, the SEM micrographs showed the appearance of bulges on the surface. The latter were then analyzed by Time-of-Flight Secondary Ion Mass Spectrometry (ToF-SIMS) to characterize their molecular composition.

The purpose of this work is to identify possible new strategies for faster identification of factors that eventually influence chemical resistance of pharmaceutical glasses, and to provide useful information needed to improve industrial processes.

1. INTRODUCTION

The chemical composition of the glass surface is influenced by various interactions which occur on the uppermost atomic layers (1), for this reason the glass surfaces could not have the same composition as the respective bulk glass. On the other hand, the surface properties of glass containers are greatly influenced by the forming process and they are not simply determined by the bulk composition (2,3). It is well known, indeed, that the high temperature, required to convert the glass tube into a container, modifies the composition of the inner surface and creates inhomogeneities in different areas of the vials (4–6). The investigation of elemental and phase composition of glass surfaces in dependence on their physical and chemical history is thus crucial to understand the reactions of glass surfaces with gases, solutions, coatings, and environmental media, and is therefore of great interest in industrial production. Numerous problems can arise by the interaction of glass surfaces especially with vapor or aqueous solutions during various steps of production, or later (7). In the pharmaceutical field, glass containers are commonly cleaned, rinsed, and then subjected to a heat sterilizing or depyrogenizing step at 120 – 400 °C directly before filling. This treatment can drastically affect the chemical properties of the outermost glass surface due to the removal of contaminants or the modification of glass composition (3,4,6,8,9). In addition, the stability of the drug solution may be compromised (10), as well as its pH value may be changed (2,9,11). One of the most common consequences for the glass surface is the alkaline degradation. Due to the interdiffusion reactions of alkali silicate glasses in aqueous solutions (12), depletion of the surface region from cations and enrichment of hydrogen content occurs. In this way, the so-called “leached layers” are formed. Thus, an extensive study of the different factors involved in forming process is essential for selecting the right actions to avoid or at least to reduce serious consequences, as well as to evaluate the chemical durability of glass.

Since borosilicate glass is still the material of choice for the primary packaging of parenteral drugs, a sophisticate study of the surface, which is directly in contact with the drug product, is important to optimize process parameters and to obtain reliable containers.

Two types of type I borosilicate glass tubes with a slightly different composition, and corresponding vials obtained from the same batches of the glass tube were analyzed using surface sensitive spectroscopic methods, such as x-ray photoelectron spectroscopy (XPS) and static time-of-flight secondary ion mass spectrometry (ToF-SIMS) techniques. XPS and ToF-SIMS were applied to obtain chemical information on the glass surface in order to support research and development activities, the optimization of processes and the control of production.

XPS provides qualitative and quantitative information on all elements of the outermost sample surface (except for H and He) in a sampling depth of 3 - 10 nm (13). The elements can be identified on sample surfaces from the binding energies (BEs) of photoelectrons emitted during x-ray excitation. Tabulations of electron binding energies of the elements enable elemental identification. In addition, one of the main advantages of XPS is the possibility of obtaining chemical information relatively easily by analyzing small shifts of the binding energy of the photoelectrons, typically lower than few eV. The relative amounts of the detected elements within the analysis volume can, in principle, be extracted from the intensities of the photoelectron peaks if the sample is assumed to be homogeneous over the XPS sampling volume. For these reasons, XPS has become one of the most widely used surface-analysis tool.

Despite the versatile fields of applications, XPS lacks detailed macromolecular information on the surface chemistry. A useful support to fill this gap is given by time-of-flight secondary ion mass spectrometry. ToF-SIMS provides information related to the chemical composition of sample surface with a depth resolution in the nanometer scale (14), together with imaging

with extreme surface sensitivity and sub-micro lateral resolution (15). ToF-SIMS is readily capable of identifying different adsorbed compounds due to its high mass resolution and chemical specificity, with detection limits on the order of 10^6 –10^8 atoms /cm^2 in inorganic samples, consequently, corrosion and contamination phenomena can be sensitively studied. Compositional changes in glass surfaces, investigated by ToF-SIMS imaging, provide information on the chemical distribution of structures and inhomogeneities (e.g., lenses, bulges, craters and holes, and precipitates) created during the vial forming process and observed by scanning electron microscopy (SEM) micrographs.

The purpose of this work is to combine two complementary surface analytical methods in order to acquire detailed information of the inner surface of glass tubing before and after the vials forming process. The use of surface techniques can better help glass manufacturers to correlate critical process parameters with container chemical behavior, since it is the outermost layer that is in direct contact with a drug product.

2. EXPERIMENTAL METHODS

Sample preparation

In the present study, two types of type I borosilicate glass tubes containing different amounts of oxide component were analyzed: A-glass and B-glass have a similar chemical composition, mainly differing for the presence of barium and potassium on B-glass. The chemical composition was measured by X-ray fluorescence spectroscopy according to DIN 51001 2003-08 norm. The results are reported in Table 1.

Table 1: Chemical composition (wt.%) *of the two glasses used in this work.*

	Chemical composition						
	SiO_2	**B_2O_3**	**Al_2O_3**	**Na_2O**	**K_2O**	**CaO, MgO, BaO**	**other**
A-glass	75.0	10.5	5.5	7.0	<0.05	1.5	<0.5
B-glass	72.0	10.5	7.2	6.0	1.9	2.1	<0.5

In addition to the glass tubes, the corresponding glass vials in format 2R, manufactured using the glass tubes of the same batch, were analyzed. The minimal differences in the manufacturing process of the two type I glass vials are dictated by the distinct viscosity curves of the two composition. The vials were picked up immediately after the annealing process: the vials have to pass through high-temperature furnaces at about 570 °C in order to reduce stress in glass walls. Before analysis, vials were rinsed with deionized water. For each glass tube and each vial, three measuring positions on inner surface were analyzed along the vertical axis. After fracturing, two glass fragments per tube and vial were considered. During the measurements, any possible effect due to the cutting process used to prepare the samples was excluded.

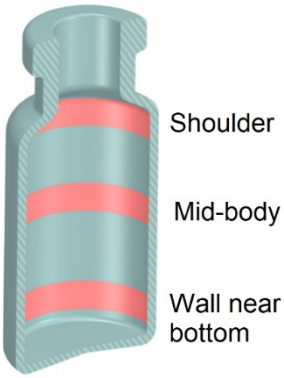

Figure 1: Area of analysis: along the vertical axis of the inner surface of the vial for the XPS analysis; the near-bottom area for SEM and ToF-SIMS analyses.

X-ray photoelectron spectroscopy

For the XPS analyses, a fragment of each sample was attached to the sample holder using double sided carbon based tape and inserted into the high-vacuum chamber of the spectrometer. The measured points were located on the inner concave surfaces of the glass tubes/vials. All work was conducted with a Kratos Analytical Axis Ultra instrument equipped with a monochromatic Al Kα (1486.6 eV) X-ray source. The angle-resolved XPS measurements were carried out in order to achieve greater surface sensitivity by simply changing the orientation of the detector to the sample normal, referred to as the angle of emission. When the sample is untilted ($\theta = 0°$), the sampling depth is approximately around 10 nm; while when the sample is tilted ($\theta = 60°$), the sampling depth is reduced to 5 nm. Thereby, a larger angle of emission enhances the signal from the surface.

Due to the insulating property of glass surfaces, an electron flood gun was applied to neutralize the net positive surface charge. Survey scans and high-resolution narrow binding energy range scans of O 1s, Na 1s, C 1s and Si 2p peaks were recorded. The value of 285.0 eV binding energy for the C 1s peak of adventitious (hydro)carbon contamination was chosen as reference for the calibration of the energy scale. We are well aware that this procedure is not completely reliable, falling that signal usually in a very large BE range (284.0–285.6 eV) depending on the material under investigation (16,17). However, the solidity of our attribution was checked by the consistence of BE values determined for the bands related to the main elements in glass (Si and O). Fitting of collected spectra was carried out by the software XPSPeak4.1, using mixed Gaussian-Lorentzian functions. Shirley backgrounds were used in all fits to narrow scan spectra. Constraints for full-width half-max (FWHM) and position of components peaks were implemented as needed. The final uncertainty on the determined BE is around 0.2 eV. Atomic concentrations were calculated by determining the integral peak intensities, with final relative uncertainty around 10% of the calculated value.

Static Time-of-Flight Secondary Ion Mass Spectrometry

ToF-SIMS analyses in the static SIMS mode were performed in a ToF-SIMS IV instrument (ION-TOF GmbH) using 25 keV Bi^{3+} primary ions and low-energy electron flooding for charge compensation. High lateral resolution spectra were acquired in collimate mode at a spatial resolution of ~1÷2 μm, over an area of about 50×50 μm^2 at 512×512 pixels.

Scanning electron microscopy

SEM analysis was performed using a Zeiss ∑igma Variable Pressure Field Emission Scanning Electron Microscope (VP-FE-SEM) with 1.5 nm of maximum resolution, in vacuum mode and using the following parameters to avoid charging artifacts: 30 mm^2 aperture, 1 keV beam energy and working distance between 2 and 4 mm.

The samples were fragmented to obtain small pieces to be inspected under SEM microscope.

3. RESULTS

Characterization by XPS

XPS was used to characterize the elemental composition and chemical environments of the glass tubes and their respective vials (for the area of analysis see Fig. 1). Survey spectra were collected before and during analysis, and were used to determine glass compositions and surface contamination. Fig. 2 shows the survey spectra of the inner surface of the glass tubes acquired at 0° emission angle.

Very small amounts of carbon are deposited on the surface of all glass samples as evident by development of a C 1s XPS peak at 285 eV binding energy and shown in Fig. 2. The C 1s peak represents adventitious carbon (AdC) which is universally present. The survey spectra of the vials (not reported here) are consistent with those collected for the glass tubes.

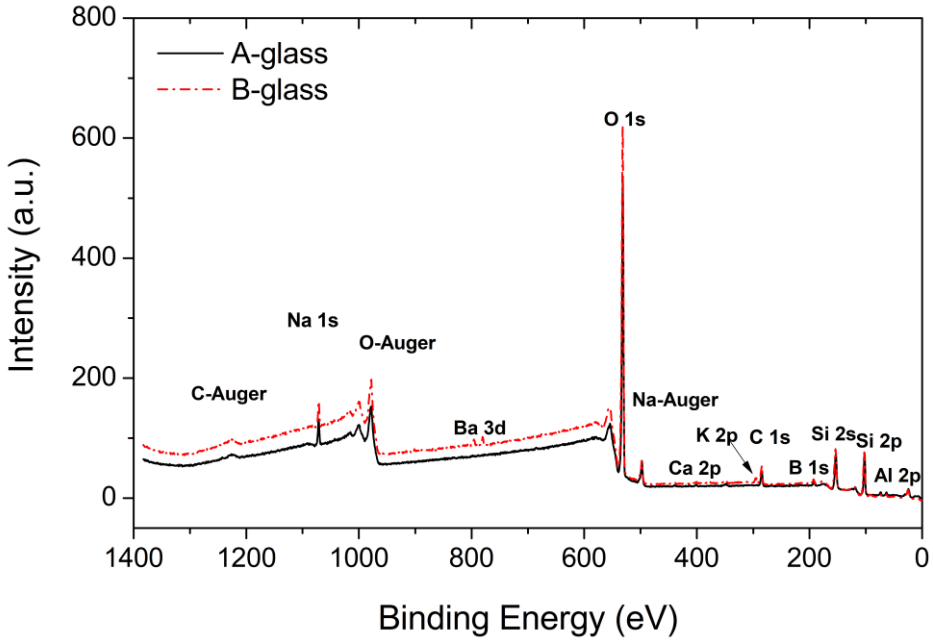

Figure 2: Survey spectra (0-1400 eV) of A-glass (black solid line) and B-glass (red dash-dotted line) tubes. Major spectral lines are labelled.

The chemical composition of glass tubes was determined by quantifying the integral of XPS high resolution spectra; the results are reported in Table 2 for two emission angles, thus for two sampling depths: i.e., about 10 nm and 5 nm. As expected for a surface contamination, at shallow sampling depth (5 nm) the relative amount of carbon is higher. The exposure of the surface to adventitious entities or contaminants, such as carbon, causes the attenuation of the signals from the other elements present in the sample, depending on the electrons inelastic mean free path through the elements under study, thus altering the measured atomic concentrations. Therefore, the direct calculation of atomic percent compositions through the simple renormalization of the data, without further correction, can give rise to misleading results. In order to address this issue, Smith (18) proposed a simple method, easy to implement, and that requires no additional data acquisition and only minimal data processing. The first step is the determination, by standard methods, of the carbon concentration on the surface. Hence, under the hypothesis that the carbon contamination is homogeneously covering the sample surface, the latter can be converted directly to an overlayer thickness in

nanometers, by the use of a modified form of the Beer–Lambert law (19). The hydrocarbon overlayer causes the preferentially attenuation of the emitted electron with higher binding energy (lower kinetic energy), thus inducing an underestimation of that element. Once evaluated the hydrocarbon contamination thickness, a more correct signal intensity, without the effect of the hydrocarbon layer, may be estimated. Finally, the resulting values of correct signal are then renormalized to 100% to obtain an estimate of the composition without the hydrocarbon contamination. The data correction can be carried under the assumption that the sample has a uniform composition within the XPS sampling depth. The hydrocarbon-corrected surface composition of the glass tubes at two emission angles are reported in Table 2, together with the apparent thickness (nm) of the hydrocarbon layer.

Table 2: Quantitative elemental composition on inner surface of two glass tubes determined by XPS at two sampling depths. Atomic concentration (at.%) after correction for the hydrocarbon contamination layer, and C thickness (nm).

			Chemical composition									
	Sampling depth		**Na**	**Ba**	**O**	**Ca**	**K**	**C**	**B**	**Si**	**Al**	**C thickness**
A-glass	10 nm		4.8		56.7	0.3		14.3	4.1	17.6	2.2	
		Hydrocarbon-corrected	6.6		66.2	0.3			4.7	19.7	2.5	0.4
	5 nm		2.8	0	57.1	0.3	0	14.2	3.3	20.0	2.3	
		Hydrocarbon-corrected	3.8	0	67.0	0.4	0	0	3.8	22.5	2.5	0.4
B-glass	10 nm		3.4	0.2	58.9	0.3	0.9	12.4	3.7	18.1	2.1	
		Hydrocarbon-corrected	4.6	0.3	67.5	0.3	1.0		4.1	19.9	2.3	0.3
	5 nm		2.4	0.2	57.2	0.3	0.9	17.0	3.3	16.8	1.9	
		Hydrocarbon-corrected	3.4	0.2	69.5	0.4	1.0		3.8	19.5	2.2	0.5

The hydrocarbon-corrected content of B, Na, K (B-glass) and Al rescaled by Si, measured on inner surface of the two glass tubes, are reported in Fig. 3, together with theoretically expected values (dashed line), evaluated according to the data shown in Table 1.

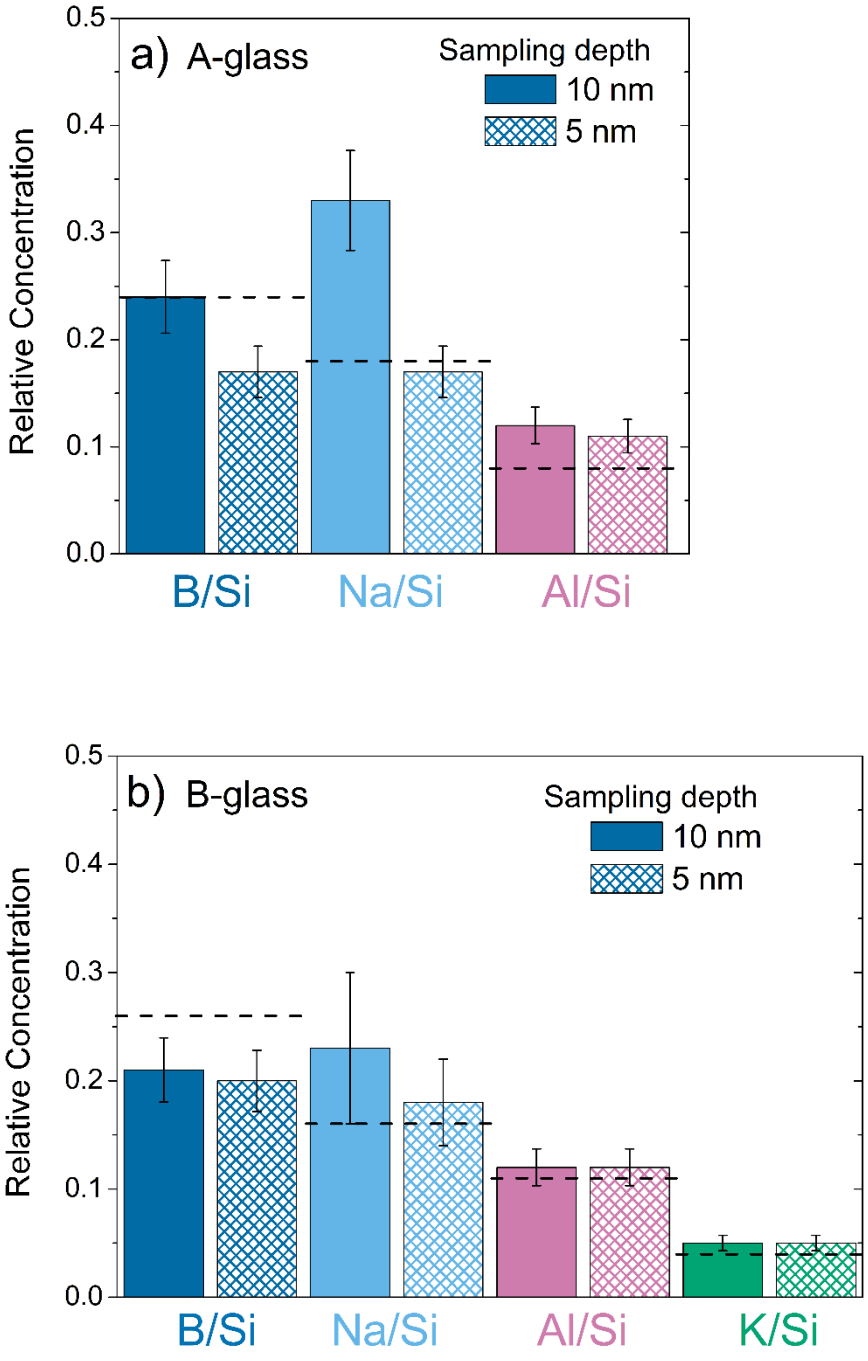

Figure 3: Hydrocarbon-corrected amount of different elements rescaled by silicon, determined by XPS at two sampling depths on inner surface of glass tubes: a) A-glass and b) B-glass. Dashed line indicates nominal value ratio.

A-glass tube shows a slight increase in sodium in the first 10 nm, if compared to the theoretically expected value (dashed line) and to the shallow depth (5 nm). Further, A-glass

shows a small increase in boron at 10 nm than at 5 nm of sampling depth, and the former value is closer to the theoretically expected.

At both sampling depths, a decreased boron content in B-glass tube was measured than the nominal amount (dashed line). On B-glass tube surface, the sodium value measured at 10 nm shows a significant standard deviation, an indication that the analyzed surface is not completely homogeneous; while the estimated value at 5 nm is compatible with the nominally expected value. The content of potassium on B-glass tube surface is the same for both sampling depths, and close to the expected value. Finally, the aluminum content is nearly the same in both sampling depth and for all glass tubes considered in this work.

The before and after hydrocarbon-corrected surface composition of the vials at 0° of emission angle are reported in Table 3, together with the apparent thickness (nm) of the hydrocarbon layer.

Table 3: Quantitative elemental composition on inner surface of two different vials determined by XPS at 10 nm of sampling depth, in three measuring regions. Atomic concentration (at.%) after correction for the hydrocarbon contamination layer, and C thickness (nm).

	Sampling area		Chemical composition									C thickness
			Na	Ba	O	Ca	K	C	B	Si	Al	
A-glass	Shoulder		9.3		58.2	0.4		9.4	3.3	17.5	1.9	
		Hydrocarbon-corrected	11.4		63.9	0.5			3.5	18.7	2.1	0.3
	Mid Body		7.4		57.9	0.4		9.8	3.4	19.2	1.8	
		Hydrocarbon-corrected	9.1		64.0	0.5			3.7	20.8	2.0	0.3
	Wall near bottom		8.3		58.2	0.6		8.8	5.0	17.2	1.9	
		Hydrocarbon-corrected	10.0		63.6	0.7			5.4	18.3	2.0	0.2
B-glass	Shoulder		7.3	0.2	56.7	0.3	0.7	9.4	5.6	17.7	2.2	
		Hydrocarbon-corrected	8.9	0.3	62.4	0.3	0.8		6.1	19.0	2.3	0.2
	Mid Body		5.7	0.2	55.9	0.3	0.8	8.5	4.5	21.4	2.8	
		Hydrocarbon-corrected	6.9	0.3	61.0	0.3	0.8		4.9	22.8	3.0	0.2
	Wall near bottom		6.6	0.2	56.2	0.3	0.8	8.0	6.3	18.5	3.0	
		Hydrocarbon-corrected	7.9	0.2	61.0	0.3	0.9		6.8	19.7	3.2	0.2

Fig. 4 shows the relative amount of B, Na, K (B-glass) and Al rescaled by Si for each vial, distinguishing between three measuring regions of the vial: shoulder, mid body and wall near bottom; which are subjected to different temperature gradients during the forming process. In order to simplify the reading, these results are reported together with those recorded in corresponding glass tubes (dashed line), remembering that in this case only one sampling depth, i.e. 10 nm, is taken into account.

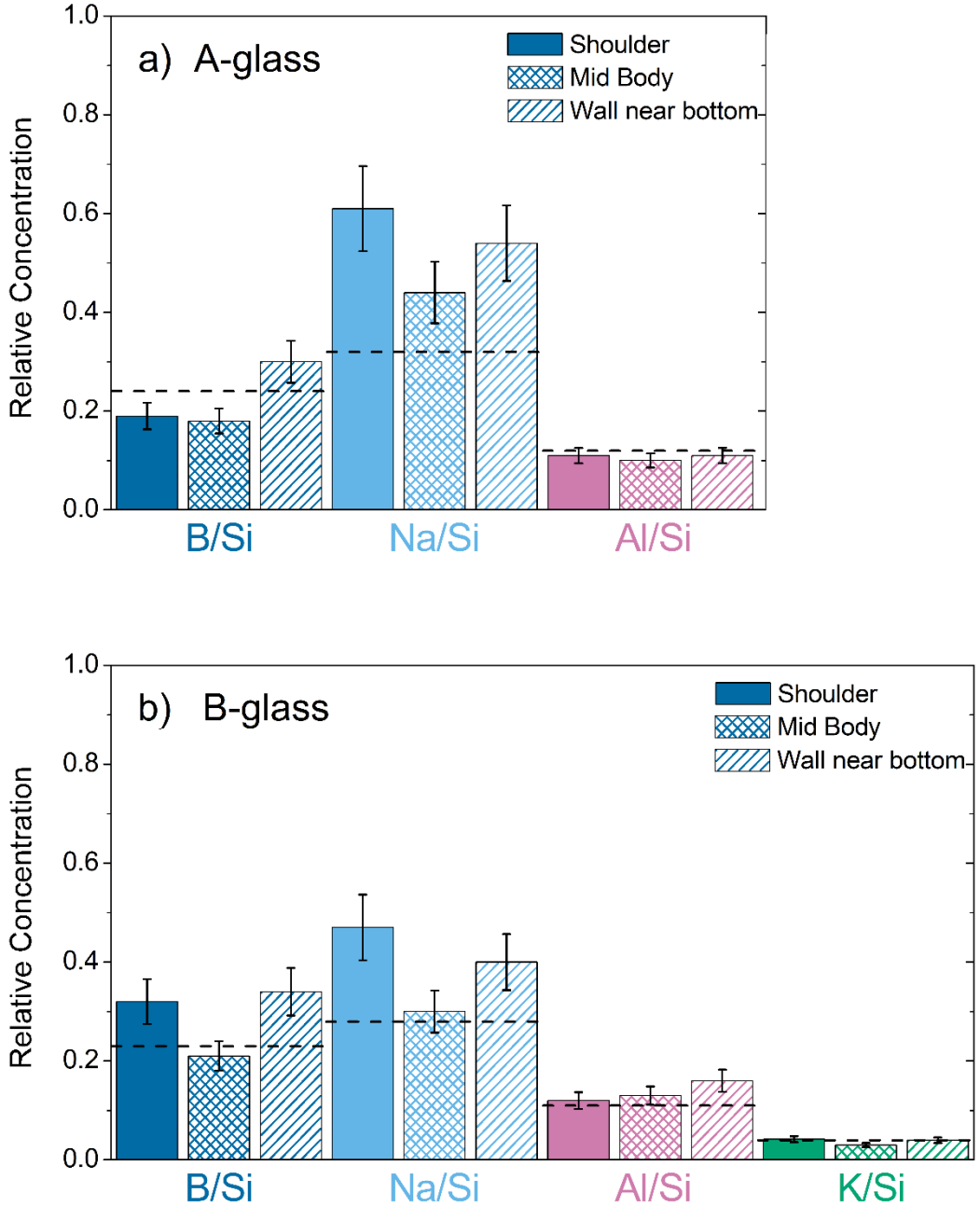

Figure 4: Hydrocarbon-corrected amount of different elements rescaled by silicon, determined by XPS at 10 nm of sampling depth on inner surface of vials: a) A-glass and b) B-glass. Dashed line indicates the ratio measured on inner surface of corresponding glass tube. Different areas of the vial are considered.

One immediately notices the increase in sodium on inner surface of vials as compared to the corresponding glass tube, especially in A-glass vial at the shoulder and wall near bottom region. Secondly, worthy of attention is boron, which shows different behavior depending on the investigated region in A-glass vial. Shoulder and mid body areas are characterized by an amount of boron close to that measured on the corresponding glass tube, whereas the wall near bottom area shows slight growth compared to the other two areas of the vial. The trend of aluminum is rather constant along the vertical axis of the vial and does not differ from the value measured on the corresponding glass tube.

The B-glass vial deserves a separate discussion. One can note even in this case a higher value of sodium amount as compared to the corresponding glass tube. However, this increase is not as marked as in the case of A-glass vial. As in the previous case, sodium accumulation is higher at shoulder and wall near bottom areas. Furthermore, in B-glass vial the behavior of boron mirrors that of sodium. The aluminum content shows the same behavior observed in the A-glass vial, but with a slight increase in the wall near bottom region. Finally, the amount of potassium is also reported: its content is nearly constant along the vial, and reflects the values measured on the corresponding glass tube.

XPS spectra shown in Figs 5, relative to glass tubes surface, are representative of all samples analyzed in this work. A typical O 1s photoelectron spectrum for type I borosilicate glass tube is shown in Fig. 5a, a result of the curve fitting is also illustrated. The fit parameters are summarized in Table 4, while the oxygen speciation is reported in Table 5. Since oxide ions in the sodium borosilicate system have different type of chemical bonding, it is possible to analyze the bonding states of oxide ions by deconvoluting the O 1s spectrum. In the experimental spectrum shown by symbols, there is a well-resolved peak around 532.5 eV that

is attributed to bridging oxygen (BO). The second lower BE peak, is derived from other types of oxygen, i.e. non-bridging oxygen (NBO). The type I borosilicate glass should have various chemical bonding, such as Si–O–Si, Si–O–B_n, B_n–O–B_n (where n = 3 or 4 means the coordination number of oxides around a boron atom) for the BO component and at least two types, Si–O–Na^+ and B_3–O–Na^+ for the NBO component (20). The FWHMs of the BO component (1.6 eV) and the NBO component (<1.5 eV) are however so small that further separation of the respective components was not feasible.

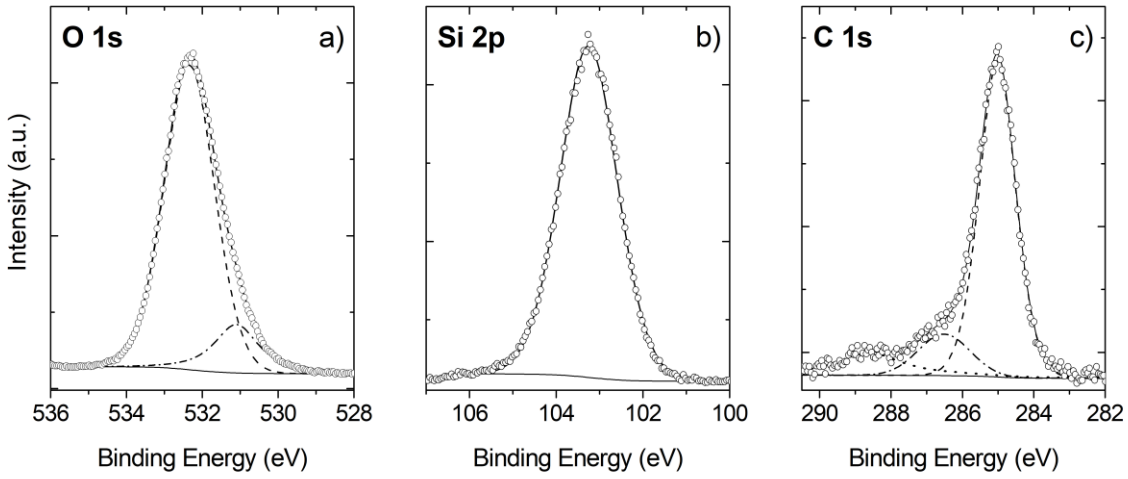

Figure 5: High resolution spectra: a) O 1s photoelectron spectrum of type I borosilicate glass tube (open symbols). The peak was fitted including the bridging oxygen (BO) (dashed line) and the non-bridging oxygen (NBO) (dash-dotted line); b) Si 2p spectrum of type I borosilicate glass tube, the fit is represented by a solid line intersecting the data points (open symbols); c) C 1s photoelectron spectrum (open symbols). The peak was fitted including C-C/C-H (AdC) (dashed line), C-O chemical bonds (dash-dotted line), and carbonate groups CO_3 (dotted line). A Shirley background is included (solid curve at base of peaks).

The chemical shift of silanol OH with respect to bridging oxygen is commonly found to be at +0.55 eV (21), thus it overlaps the bridging oxygen signals, and a reliable assignment is not possible (21,22). It may be identified, however by line broadening (>1.5 eV) of the BO peak. Therefore, the surface of glass tubes may contain hydrous species in addition to NBO and BO. The hydrous species observed in O 1s spectra are typically considered as a combination

of surface hydroxyls and water, as a distinction cannot be made without removal of physisorbed water at elevated temperatures (21). Experiments have proved that the hydrous species result as a consequence of an interdiffusion reaction with the cations of the glass (21).

Table 4: Peak parameters derived from fitting XPS spectra acquired at 10 nm of sampling depth on inner surface of glass tubes: O 1s, B 1s, Na 1s and Si 2p (BE and full width half maximum (FWHM) in eV).

	O 1s		***B 1s***	***Na 1s***	***Si 2p***
	BO	NBO			
A-glass	532.5 (1.6)	531.2 (1.2)	193.1 (1.6)	1072.1 (1.7)	103.2 (1.6)
B-glass	532.5 (1.8)	531.2 (1.5)	193.1 (1.5)	1072.0 (1.7)	103.2 (1.6)

Table 5: Speciation of oxygen determined using O 1s peak fit acquired at 10 nm of sampling depth on inner surface of glass tube and after the correction for the hydrocarbon contamination layer.

	BO	**NBO**	**NBO/BO**
	(at. %)	(at. %)	
A-glass	59.0	7.0	0.12
B-glass	57.4	6.9	0.12

Si 2p experimental result is illustrated in Fig. 5b. The spectrum is fitted with one Si 2p spin-orbit split doublet (the Si $2p_{3/2}$ and Si $2p_{1/2}$ peaks). The fit parameters are summarized in Table 4. The C 1s band is shown in Fig. 5c. It can be resolved into the C-C/C-H line, fixed at 285.0 eV, the line at 286.2 eV attributed to C-O group and the line observed at 288.5 eV, suggesting a possible formation of carbonates.

Table 6 contains the relative content of BO and NBO species for the vials.

Table 6: Speciation of oxygen determined using O 1s peak fit for glass surfaces of vials, and after the correction for the hydrocarbon contamination layer.

	BO	NBO	NBO/BO
	(at. %)	(at. %)	
A-glass	55.5	8.1	0.15
B-glass	54.2	7.3	0.12

Finally, Fig. 6 shows the C 1s and Na 1s spectra measured in B-glass vial and in the corresponding glass tube. It is notable that the contribute of the carbonate components at >288 eV, measured on inner surface of the vial (blue triangles), is much greater than that acquired on the glass tube (black squares). Furthermore, comparing the two spectra of sodium line, one can note a distinct shift to lower energy of Na 1s peak measured in the vial. Fig. 6 shows the specific case of B-glass samples, but this phenomenon was observed also in A-glass vial and the respective tube.

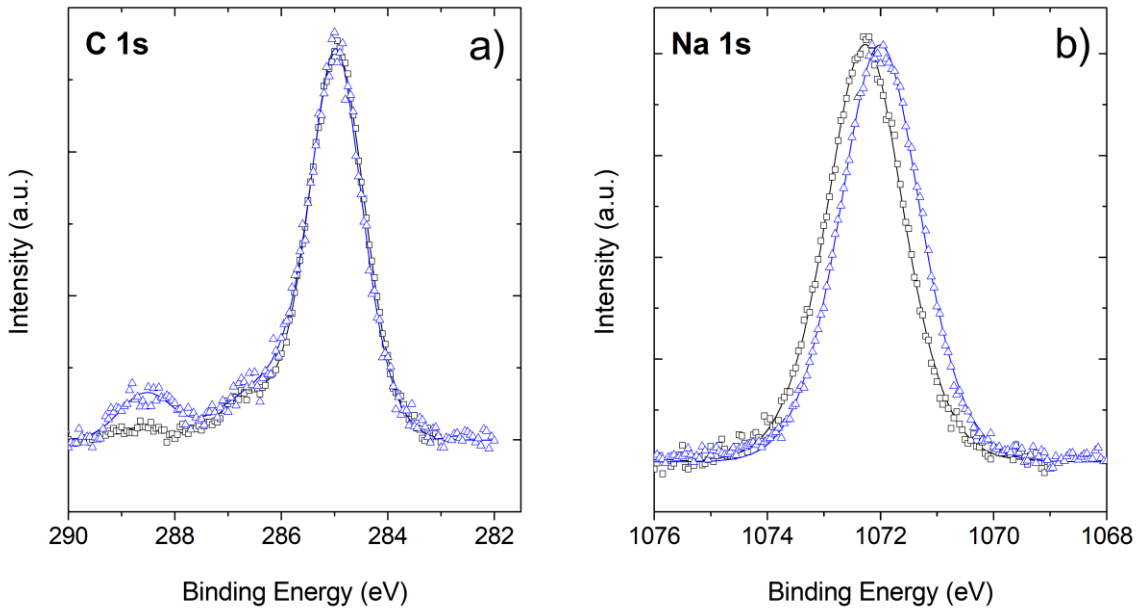

Figure 6: a) High-resolution C 1s photoelectron spectra, and b) high-resolution Na 1s photoelectron spectra acquired on the inner surface of the B-glass tubing (black symbols) and vial (blue symbols).

SEM and ToF-SIMS characterization

Surface morphology of the inner glass surface was observed by SEM analysis. The selected areas of analysis for vial (see Fig. 1) were the lower part, which is usually the area most prone to glass corrosion when in contact with the drug product solution, the mid-body and the shoulder.

The surface of pharmaceutical containers obtained by tubing is affected by the converting process. The glass tube is subjected to the action of multiple high-temperature flames which are aimed to cut the tube, forming the bottom, and shaping the neck of the vial. During these steps, depending on the speed of the forming machine and flames temperature, alkali borates evaporate from the hottest region and condensate or diffuse-in the coldest surface regions (5). The effect of this phenomenon is morphologically visible over the inner surface of the vial (only the results of one vial are reported because representative of both glass tubes). Fig. 7 is a comparison between the glass tube morphology and the related vial at different regions after the converting process: the so-called bulges from alkali borates are visible in the vial surface.

The wall near bottom area was analyzed by ToF-SIMS mapping to characterize its chemical composition. The images, reported in Fig. 8 related to one vial are representative of both glass tubes. Maps clearly show that the distribution of B is related to Na, suggesting that B is chemically bonded to Na. In particular, the ion $Na_2BO_2^+$ (both isotopes ^{10}B and ^{11}B) is the most intense molecule showing the distribution of the bulges as observed in the SEM micrograph.

The maps show the distribution intensities of the reported elements. While they are proportional to the concentration, the conversion factor to concentration values (relative sensitivity factor) depends on the element. This explains why Si^+ image, for example, is less intense compared to Na^+.

Tof-SIMS imaging is a powerful technique that can give a general overview of what type of species, at lower levels, are present on the surface. However, the analysis of these bulges was difficult for the limited optical capabilities of the technique making difficult to identify the sampling area/region of interest.

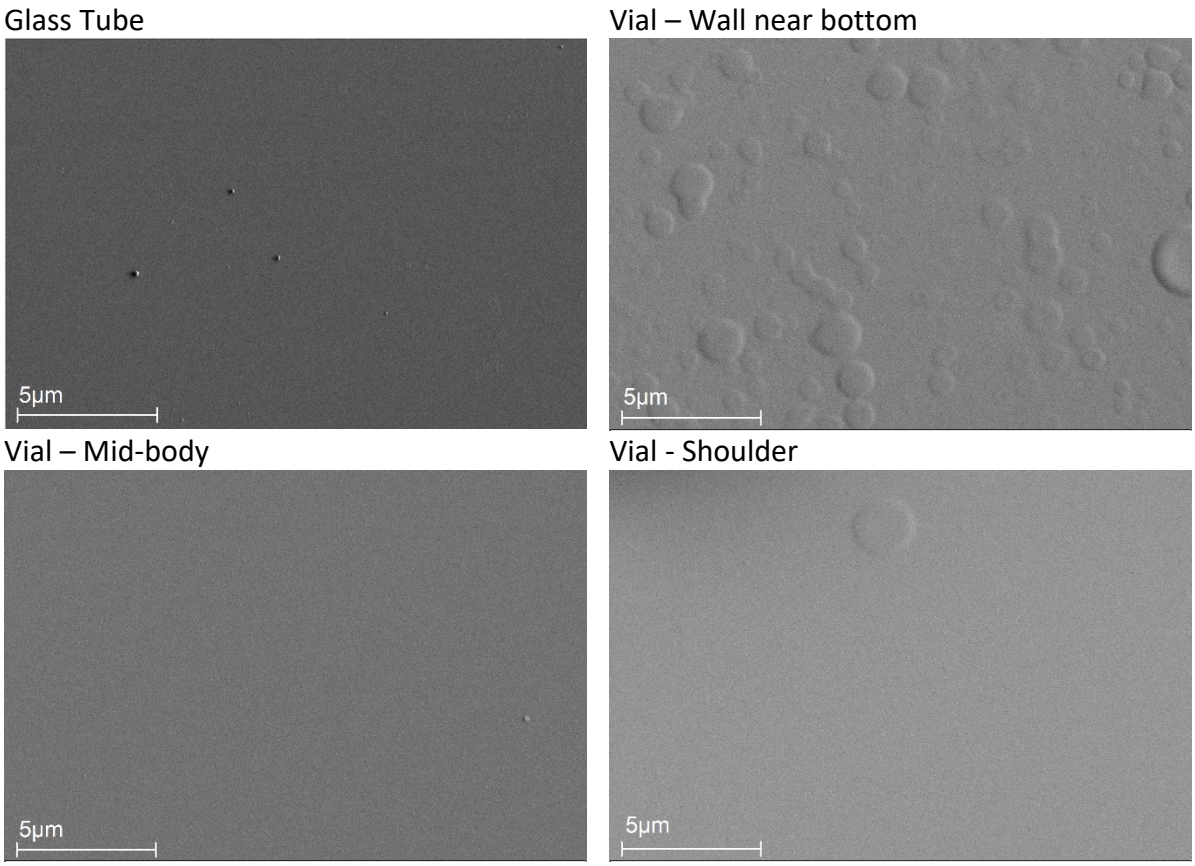

Figure 7: SEM micrographs of the inner surface of glass tubing, and the related vial at different regions.

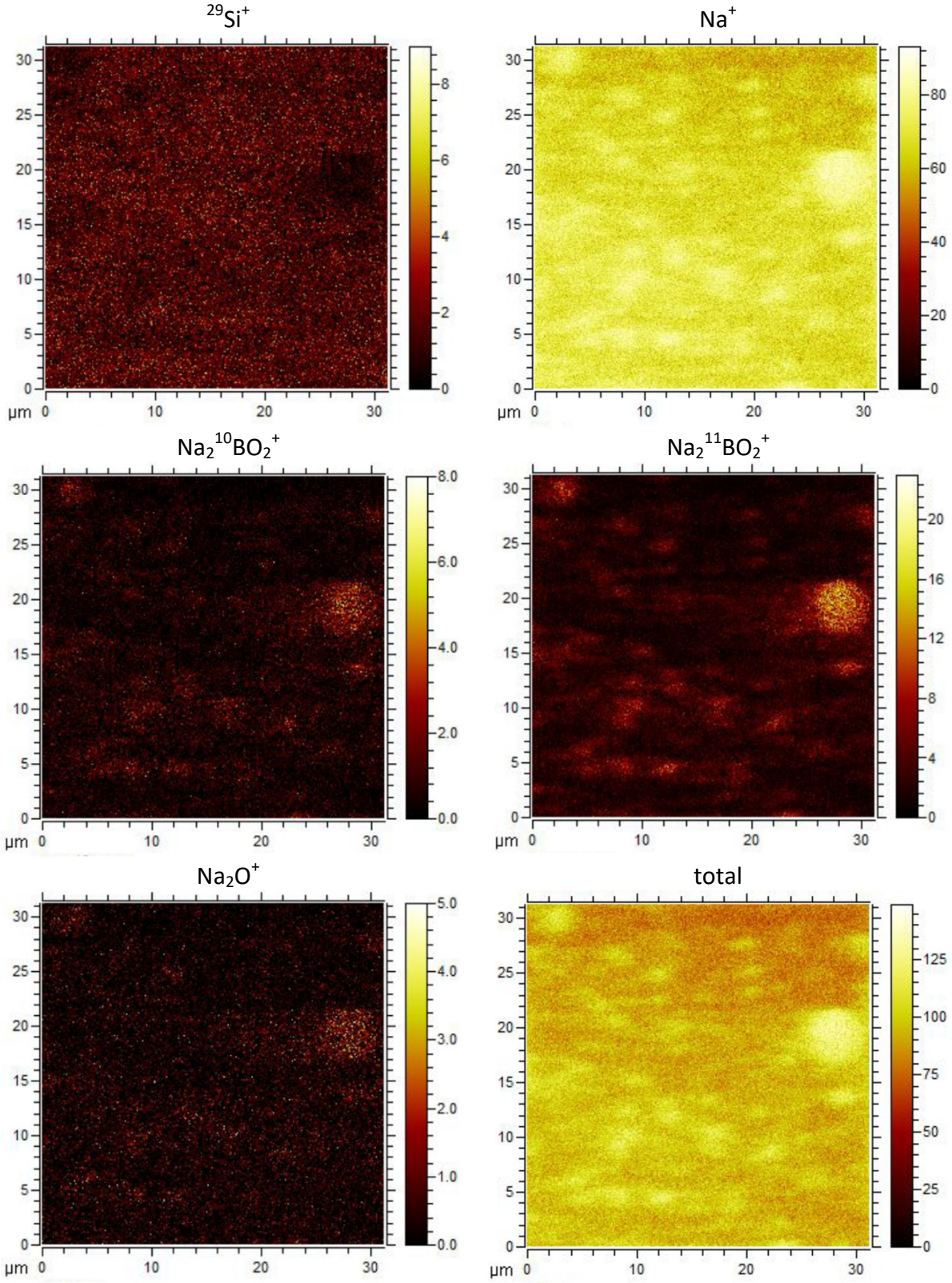

Figure 8: ToF-SIMS images of inner surface of wall near bottom of the vial after the forming process (field of view: 30×30 µm^2). The lateral resolution is about 1 µm.

4. DISCUSSION

Due to the manufacturing process of both, glass tube and container, the surface of the glass exhibits a different composition than the bulk material, as revealed by the XPS analyses.

The two glass tubes A-glass and B-glass have a similar composition, but they are characterized by a different concentration of network former (boron, silicon, and aluminum) and by the presence of potassium and barium in B-glass. These differences, apparently small, may have macroscopic effects on the corresponding chemical properties of glass: e.g., the mobility of an alkali ion is reduced when another alkali ion is added, this is associated to the "mixed-alkali" effect (23,24). The mechanism of this effect is still debated, however, it could explain the different behavior of sodium on the inner surface of the A-glass tube. The relative amounts of sodium and boron measured at two different sampling depths, change in a sensible manner on A-glass tube, while they remain constant on B-glass tube. The Na decrease, measured at the uppermost surface layer of the first glass, may be due to the interdiffusion of the alkali ion that may take place in contact with water vapor (25–27). Whereas, the ion exchange reaction is partially hindered in the second glass tube due to the mixed-alkali effect. The boron decrease, observed in the first 5 nm of the A-glass tube, is probably due to the high volatility of this ion (6,11,28). In B-glass tube, this drop seems to extend to the first 10 nm. The difference between the two glass tubes may be attributed, again, to their different composition.

Obviously, the mixed-alkali effect may also influence properties of the final container. Indeed, two containers of different glass composition, obtained through a similar forming process, can show different chemical properties (29). The slight increase in sodium, detected on the inner surface of vials, is partially due to volatile species generated from the bottom area during the forming process, which condense on the inner glass surface of the vial due to

the lower temperature along the vial wall. The condensation process leads to an inhomogeneous coating of the inner walls with typical evaporation deposits like sodium borates (3,8,30). Probably, during the rinsing step, the condensed species are partially removed from the surface. This explains why an increase in boron, proportional to that of sodium, is not observed.

XPS provides an insight into the compositional changes in the top 10 nm of the vial glass surface, thus the measured increased of sodium can be related also to another contribution. ToF-SIMS analyses revealed that the bulges are mainly sodium borates, but XPS analyses show no comparable growth of boron. This suggests that there are two contributions to sodium accumulation at the surface: the first comes from the deposition of condensed species, the second can be related to the high mobility that characterizes the alkali ion but not boron. The annealing process can induce the sodium diffusion from the bulk towards the surface, thus justifying the difference between the relative amount of the two elements. In addition, the regions showing the most significant Na increase are, in both vials, the shoulder and the region near the vial bottom. Further investigation would be needed to explain this result. However, it can be assumed that the flames used during the forming process, for the shoulder and the bottom parting, may facilitate the diffusion of the alkali ion from the bulk. Finally, the differences recorded on the B-glass vial, compared to the A-glass, can be attributed to the mixed-alkali effect, which as mentioned before influence the alkali ions mobility.

In this work the surface oxygen speciation was established by fitting the O 1s spectra. Two distinct peaks are resolved: the lowest BE peak includes the NBO signals, while the highest BE includes all BO signals. It is interesting to note that the BO/NBO-ratio remains quite constant over glass tubes and corresponding vials, see Table 5 and Table 6. This finding seems to be in contrast to the increase in surface Na concentration measured on the inner surface of the vial. However, one can assume that Na species that condense or diffuse towards

the surface cannot cause significant changes in the glass network structure and hence the BO/NBO-ratio. In addition, the distinct shift of the Na 1s core level state towards lower BEs indicates that a low portion of Na on the vial surface could be involved in carbonate formation: XPS proofs the presence of some carbonate phases on both glass tubes and vials, with an appreciable increase in the latter case. The Na 1s BEs on the surface of the vial approach the value reported in the literature for $NaCO_3$ (31). The presence of carbonate phases in the C 1s signal can be an indication of an early stage of corrosion that is occurring on glass surface, probably due to the vapors or combustion pollutants to which these products were exposed, during the forming process.

The volatile species, that condense on the inner surface during the vial forming process, typically form small, round sodium borate adsorbate bulges (11). SEM figures showed a wide distribution of bulge structures, the morphology of which changes with increasing distance from the bottom along the axis of the vial. These compounds are possibly sodium borate, as confirmed by ToF-SIMS analyses, which show a distribution of these species compatible with that observed with SEM. ToF-SIMS provides the mapping of mass fragments of elements and molecules that constitute these structures. In other words, the surface composition can be inferred by considering that the spectrum acquired during ToF-SIMS analysis is the result of the interaction of the primary ion beam and the molecules on the surface. Indeed, the original molecule that generate the bulges could be an impurity from the original raw material, such as sodium tetraborate decahydrate (32).

Na^+ map confirmed the XPS results since this ion is mainly concentrated on the surface. It should be stated that in the collected data, other ion elements are present, not showed in this study that can be extracted by a retrospective analysis, for example Na_2BO_3H.

5. CONCLUSION

Chemical analyses over glass surfaces were performed by XPS, SEM and static ToF-SIMS. The utilization of these highly sensitive surface analytical techniques provides further information on the outer glass container layer and they can help to understand mechanism/process and kinetic events that can occur during the shelf life of a pharma drug product.

In the present study, XPS provided quantitative information on the chemical states of elements such as oxygen (OH, NBO, BO). In addition, angle-resolved XPS guaranteed greater surface sensitivity by simply tilting the sample. Thanks to this technique, the change in the relative concentration of volatile species, such as boron and sodium, from the expected value of the bulk was shown, thus revealing the effects of ion exchange and enrichment of ions on the surface. Moreover, it has been demonstrated that the impact of the vial-forming process is not limited to topological effects, but produces changes that extend to at least the first 10 nm of the surface, and these changes may depend on the investigated region. On the other hand, SEM proved to be the most immediate tool to reveal the variation in surface morphology, and thus allowed us to identify the region of the vial of greatest interest to conduct the ToF-SIMS analysis. Finally, ToF-SIMS was able to shed light on the molecular composition of the bulges observed by SEM.

Basic research on glass surface chemistry can be very helpful in developing knowledge and understanding that could feed into industry “Quality by Design” approaches. It is the surface, the outermost layer of a solid material that will really define the physico-chemical behavior of a container. Surface analysis can be used to study delamination phenomenon and corrosion, treatments of glass after manufacture (e.g., exposure to moisture), specific formulations interaction (e.g., pH effect and buffer systems), wettability (e.g., fogging effect) but even to

consider and study the critical process parameters related to a product and develop a better concept of designing and testing.

Acknowledgments

The authors would like to thank for XPS and ToF-SIMS analyses, MNF laboratory - Center for Sensors and Devices, Fondazione Bruno Kessler (TN) and in particular Roberto Canteri and Lia Vanzetti for constructive discussion in the interpretation of the results.

REFERENCES

1. Bansal NP, Doremus RH. Handbook of Glass Properties. Academic P. Orlando; 1986.

2. Ennis RD, Pritchard R, Nakamura C, Coulon M, Yang T, Visor GC, et al. Glass Vials for Small Volume Parenterals: Influence of Drug and Manufacturing Processes on Glass Delamination. Pharm Dev Technol [Internet]. 2001 Jan 31;6(3):393–405. Available from: http://www.tandfonline.com/doi/full/10.1081/PDT-100002248

3. Iacocca RG, Allgeier M. Corrosive attack of glass by a pharmaceutical compound. J Mater Sci [Internet]. 2007 Feb 1;42(3):801–11. Available from: http://link.springer.com/10.1007/s10853-006-0156-y

4. Schwarzenbach MS, Reimann P, Thommen V, Hegner M, Mumenthaler M, Schwob J, et al. Topological structure and chemical composition of inner surfaces of borosilicate vials. PDA J Pharm Sci Technol. 2004;58(3):169–75.

5. Rupertus V, Hladik B, Rothhaar U, Scheumann V. A quick test to monitor the delamination propensity of glass containers. PDA J Pharm Sci Technol [Internet]. 2014 Jul 1;68(4):373–80. Available from: http://journal.pda.org/cgi/doi/10.5731/pdajpst.2014.00990

6. Ditter D, Mahler H-C, Roehl H, Wahl M, Huwyler J, Nieto A, et al. Characterization of surface properties of glass vials used as primary packaging material for parenterals. Eur J Pharm Biopharm [Internet]. 2018 Apr;125(October 2017):58–67. Available from: https://doi.org/10.1016/j.ejpb.2017.12.018

7. Guadagnino E, Zuccato D. Delamination Propensity of Pharmaceutical Glass Containers by Accelerated Testing with Different Extraction Media. PDA J Pharm Sci Technol [Internet]. 2012 Mar 1;66(2):116–25. Available from: http://journal.pda.org/cgi/doi/10.5731/pdajpst.2012.00853

8. Iacocca RG, Toltl N, Allgeier M, Bustard B, Dong X, Foubert M, et al. Factors affecting the chemical durability of glass used in the pharmaceutical industry. AAPS PharmSciTech. 2010;11(3):1340–9.

9. Zhao J, Lavalley V, Mangiagalli P, Wright JM, Bankston TE. Glass Delamination: a Comparison of the Inner Surface Performance of Vials and Pre-filled Syringes. AAPS PharmSciTech [Internet]. 2014 Dec 18;15(6):1398–409. Available from: http://link.springer.com/10.1208/s12249-014-0167-y

10. Watkins MA, Iacocca RG, Shelbourn TL, Dong X, Stobba-Wiley C. Impact of glass corrosion on drug substance stability. J Pharm Sci. 2014;103(8):2456–63.

11. Cerdan-Diaz J, Choju K, Flynn CR, Gavioli L, Iacocca R, Meysner A, et al. Delamination Propensity of Glass Containers for Pharmaceutical Use: A Round Robin Activity Looking for a Predictive Test. PDA J Pharm Sci Technol [Internet]. 2018;72(6):553–65. Available from: http://journal.pda.org/lookup/doi/10.5731/pdajpst.2018.008599

12. Bunker BC. Molecular mechanisms for corrosion of silica and silicate glasses. J Non Cryst Solids [Internet]. 1994 Nov;179(C):300–8. Available from:

https://linkinghub.elsevier.com/retrieve/pii/0022309394907080

13. Pintori G, Cattaruzza E. XPS/ESCA on glass surfaces: A useful tool for ancient and modern materials. Opt Mater X [Internet]. 2022;13:100108. Available from: https://doi.org/10.1016/j.omx.2021.100108

14. Benninghoven A. Chemical Analysis of Inorganic and Organic Surfaces and Thin Films by Static Time-of-Flight Secondary Ion Mass Spectrometry (TOF-SIMS). Angew Chemie Int Ed English. 1994;33(10):1023–43.

15. Adriaens A, Van Vaeck L, Adams F. Static secondary ion mass spectrometry (S-SIMS) part 2: Material science applications. Mass Spectrom Rev. 1999;18(1):48–81.

16. Greczynski G, Hultman L. X-ray photoelectron spectroscopy: Towards reliable binding energy referencing. Prog Mater Sci [Internet]. 2020;107(July 2019):100591. Available from: https://doi.org/10.1016/j.pmatsci.2019.100591

17. Greczynski G, Hultman L. The same chemical state of carbon gives rise to two peaks in X-ray photoelectron spectroscopy. Sci Rep [Internet]. 2021 Dec 27;11(1):11195. Available from: https://doi.org/10.1038/s41598-021-90780-9

18. Smith GC. Evaluation of a simple correction for the hydrocarbon contamination layer in quantitative surface analysis by XPS. J Electron Spectros Relat Phenomena [Internet]. 2005 Jul;148(1):21–8. Available from: https://linkinghub.elsevier.com/retrieve/pii/S036820480500335X

19. Swinehart DF. The Beer-Lambert Law. J Chem Educ [Internet]. 1962 Jul 1;39(7):333. Available from: https://pubs.acs.org/doi/abs/10.1021/ed039p333

20. Miura Y, Kusano H, Nanba T, Matsumoto S. X-ray photoelectron spectroscopy of sodium borosilicate glasses. J Non Cryst Solids. 2001;290(1):1–14.

21. Sprenger D, Bach H, Meisel W, Gütlich P. XPS study of leached glass surfaces. J Non Cryst Solids. 1990;126(1–2):111–29.

22. Nesbitt HW, Bancroft GM. High resolution core- and valence-level XPS studies of the properties (structural, chemical and bonding) of silicate minerals and glasses. Rev Mineral Geochemistry. 2014;78(1971):271–329.

23. Isard JO. The Mixed Alkali Effect in Glasses. J Non Cryst Solids [Internet]. 1969 Aug;1(3):235–61. Available from: http://doi.wiley.com/10.1111/j.1151-2916.1965.tb14784.x

24. Doremus RH. Mixed-Alkali Effect and Interdiffusion of Na and K Ions in Glass. J Am Ceram Soc [Internet]. 1974 Nov;57(11):478–80. Available from: https://onlinelibrary.wiley.com/doi/10.1111/j.1151-2916.1974.tb11395.x

25. Doremus RH, Mehrotra Y, Lanford WA, Burman C. Reaction of water with glass: influence of a transformed surface layer. J Mater Sci [Internet]. 1983 Feb;18(2):612–22. Available from: http://link.springer.com/10.1007/BF00560651

26. Sprenger D, Bach H, Meisel W, Gütlich P. Quantitative XPS analysis of leached layers on optical glasses. Surf Interface Anal [Internet]. 1993 Aug;20(9):796–802. Available from: http://doi.wiley.com/10.1002/sia.740200908

27. Kojima G, Matsumoto K, Sakamoto O, Yamamoto Y, Kawamoto M. Interaction of water with glass at very high temperature under dynamic condition and the properties of the obtained glass surface. J Non Cryst Solids. 2001;292(1–3):50–8.

28. Nanba T, Nishimura M, Miura Y. A theoretical interpretation of the chemical shift of 29Si NMR peaks in alkali borosilicate glasses. Geochim Cosmochim Acta. 2004;68(24):5103–11.

29. Panighello S, Pinato O. Investigating the effects of the chemical composition on glass corrosion: A case study for type i vials. PDA J Pharm Sci Technol. 2020;74(2):185–200.

30. Schaut RA, Peanasky JS, DeMartino SE, Schiefelbein SL. A New Glass Option for Parenteral Packaging. PDA J Pharm Sci Technol [Internet]. 2014 Sep 1;68(5):527–34. Available from: http://journal.pda.org/cgi/doi/10.5731/pdajpst.2014.00998

31. Moulder JF. Handbook of X-ray Photoelectron Spectroscopy. Physical Electronics Division, Perkin-Elmer Corporation 1992, editor. 1992.

32. Guadagnino E, Guglielmi M, Nicoletti F. Glass: The best material for pharmaceutical packaging. Int J Appl Glas Sci [Internet]. 2022 Jul 27;13(3):281–91. Available from: https://onlinelibrary.wiley.com/doi/10.1111/ijag.16559